Study on the Local Corrosion in Aluminium Composites Reinforced with Titan and Zinc Fabricated by Friction Stir Processing

Vanya DYAKOVA [1, 2] *, Yoanna KOSTOVA [1], Christo KONDOFF [1], Plamen TASHEV [1]

[1] *Institute of Metal Science, Equipment and Technology with Hydro-and Aerodynamics Centre "Acad. A. Balevski" at Bulgarian Academy of Sciences, 67 Shipchenski Prohod Street, 1574 Sofia, Bulgaria*
[2] *National Center for Mechatronics and Clean Technologies, 8 "Kliment Ohridski" Blvd., building 8, 1756 Sofia, Bulgaria*

http://doi.org/10.5755/j02.ms.42078

Received 14 July 2025; accepted 18 November 2025

The effect of titanium- and zinc reinforcing particles in aluminum composites on the development of local corrosion was investigated. Two types of alloy A6061 T6-based composites reinforced with 2, 4, and 6 mass % Ti and Zn respectively, were fabricated by friction stir processing (FSP). The microstructure and the phase content were studied by SEM, EDS, and XRD. Intergranular (IGC) and pitting corrosion (PC) susceptibility tests were performed. IGC corrosion resistance was evaluated by standardized methods and metallographic observations. The results showed that Zn- and Ti reinforced composites were resistant to IGC. The results of cyclic polarization corrosion tests showed that alloy A6061 T6-based composites reinforced with Zn and Ti particles were susceptible to pitting corrosion. The reference alloy A6061 T6 is the most resistant to pitting corrosion and has the lowest corrosion potential Ecorr, compared to Ecorr of the composites reinforced with 2 and 6 mass % Ti. The composite reinforced with 6 mass % Zn is the most susceptible to pitting corrosion.
Keywords: aluminum composite, corrosion, friction stir processing.

1. INTRODUCTION

Aluminum matrix composites (AMCs) reinforced with fibers, particles, or filaments [1] have certain advantages over conventional metals, such as higher strength, hardness, wear resistance, and thermal conductivity [2, 3], which are essential for their durability, especially in applications where they are subjected to high temperatures, speeds, or heavy loading [4 – 6]. Nevertheless, there are cases where the use of AMCs is limited due to the complex fabrication process and the relatively high cost [2].

The technologies for friction stir processing (FSP) [3, 7 – 10] and friction stir welding (FSW) [11, 12] are applied to fabricate AMCs due to the excellent opportunities for in-situ fabrication of composite materials and their joining in non-detachable joints. FSP is appropriate for selective alloying of metals and for improving some local specific properties. In the case of FSP, composites are fabricated in the plastic state of the metal, thus avoiding some of the disadvantages of the melting process, namely the formation of coarse-grained anisotropic structures and brittle metastable phases [13].

The effect of the type, size, shape, distribution, and orientation of the reinforcing particles on the mechanical properties of AMCs has been the subject of various studies [12 – 17]. In aluminum composites with Ti reinforcing particles fabricated by FSP, an increase in strength of the material was observed without a decrease in the ductility, which is explained by the uniform distribution of Ti particles and their strong bond with the aluminum matrix [14]. It was found that in an Al-based composite with Zn particles fabricated by multi-pass FSP process [15] the hardness in the zone of stirring was significantly improved compared to the reference metal. The segregated Zn particles at the grain boundaries restrict their excessive growth and favor the development of microstructure with fine equiaxed grains.

The initial objective of this study was to investigate the influence of Ti and Zn reinforcing particles on the mechanical properties and wear resistance of alloy A6061 T6-based AMCs obtained by FSP. However, in the process of research, the authors found that there is not sufficient amount of published data on the influence of different types of reinforcing particles on the corrosion resistance of AMCs based on one type of alloy obtained by FSP [18 – 20]. So the authors set the goal to supplement the existing research on the influence of Ti and Zn reinforcing particles on the mechanical properties of alloy A6061 T6-based AMCs obtained by FSP with research on the influence of Ti and Zn reinforcing particles on the corrosion behavior of such AMCs.

2. MATERIALS AND METHODS

2.1. Materials

Alloy A6061 T6-based composites (1 % Mg, 0.63 % Si, 0.19 % Cu, 0.06 % Cr, 0.09 % Mn, 0.31 % Fe, 0.12 % Zn, and balance Al) reinforced with Zn and Ti particles with sizes of 120 μm and 44 μm, respectively, were obtained by FSP. Zinc was chosen as a reinforcing element because of its high solid solubility (82.8 mass % at 381 °C), which is the highest among the alloying metals. Besides, the interaction between Zn and Al is weak, and no intermetallic phases are formed. Zinc improves the sliding along the Al grain boundaries, and the fine-grained Al-Zn alloys exhibit

* Corresponding author: V. Dyakova
E-mail: *v_diakova@ims.bas.bg*

high ductility both at ambient and elevated temperatures [21]. On the other hand, the Ti-alloyed aluminum alloys have improved specific strength and resistance to oxidation and burning.

The technological process for the fabrication of composites by FSP is described in detail in our previous publications [22, 23]. Zn and Ti reinforcing particles were introduced into holes with a diameter of 2 mm and a depth of 2 mm in A6061 T6 plates measuring 200 × 100 × 12 mm. These plates were then subjected to FSP. The FSP tool consisted of a threaded conical pin with three grooves and a shoulder. The pin dimensions were as follows: base diameter 5.5 mm, tip diameter 4 mm, length 4 mm and shoulder diameter 13 mm. One FSP pass was performed with the following parameters: a tool rotation speed of 900 rpm and a linear speed of 60 mm/min. The maximum temperature, as measured by thermocouples at the boundary of the stirring zone, was 374.6 °C.

The quantities of Zn or Ti reinforcing powders to fill one hole are pre-calculated, and the desired concentration of reinforcing particles in the composite is achieved by varying the number of holes. The plates with reinforcing particles were subjected to FSP. Test specimens for corrosion tests with dimensions of 25 × 10 × 4 mm were cut by water cooling both from the FSP-ed plates and the reference plate of alloy A6061 T6.

Three types of sample plates were prepared: 1) samples of alloy A6061 T6 without reinforcing particles, denoted BA; 2) samples of alloy A6061 T6-based composites containing 2 %, 4 %, and 6 % Ti reinforcing particles, denoted CTi2, CTi4, CTi6, respectively; 3) samples of alloy A6061 T6-based composites containing 2 %, 4 %, and 6 % Zn reinforcing particles, denoted CZn2, CZn4, CZn6, respectively.

2.2. Characterisation methods

To characterize the microstructure and phase content of the fabricated composites with different concentrations of Ti and Zn, scanning electron microscopy (SEM) and X-ray diffraction (XRD) methods were used. The microstructure was observed using a HIROX SH-5500P scanning electron microscope with EDS microanalysis system QUANTAX 100 Advanced-Bruker in the secondary electrons mode. The phase content was determined through XRD analysis using Bruker D8 Advance powder X-ray diffractometer (Karlsruhe, Germany) with Ni-filtered Cu Kα radiation and LynxEye solid-state position-sensitive detector. The PDF-2 (2021) database package of the International Center for Data Diffraction (ICDD) and the DiffracPlusEVA software v.4.0 (Bruker AXS 2010-2014, Karlsruhe, Germany) were also applied to perform the phase analysis.

2.3. Corrosion test methods

To study the corrosion behavior of A6061 T6-based composites, an intergranular corrosion (IGC) test according to ASTM G67 and pitting corrosion (PC) susceptibility test were carried out.

2.4. Intergranular corrosion test

The total surface area of each test specimen was calculated before the IGC test. The specimens were cleaned by immersion in 5 % NaOH solution at 80 °C for 1 minute and rinsed with water. The specimens were then immersed in diluted HNO_3 for 30 seconds, rinsed, and air-dried. After the preparation, the specimens are weighed with an accuracy of ± 0.1 mg and immersed in concentrated HNO_3 at 30 °C for 24 hours. After the test, the specimens were rinsed with water and brushed to remove any adhering particles. Then the specimens were weighed again, and the mass loss [$mg.cm^{-2}$] was calculated. The corrosion resistance of each type of composite was evaluated according to Standard ASTM G67.

Metallographic analysis of the specimens was performed after the IGC testing. The cross-sections of the tested surfaces were observed, and the depth of penetration of corrosion changes was determined.

2.4. Pitting corrosion test

To study the pitting corrosion susceptibility of AMCs reinforced with Ti and Zn, cyclic potentiostatic corrosion tests were carried out in a three-electrode cell with 3.5% water solution of NaCl at room temperature. The working electrode with a surface of 1 cm^2 was fabricated from the tested specimen. Ag/AgCl was used as the reference electrode and a standard Pt sheet electrode was used as counter electrode. AUTOLAB PG204 potentiostat and NOVA 2.1 software were used. The open circuit potential (OCP) was determined. The potentiodynamic curves were recorded in scan range from -0.5 V to + 1.0 V with a scan rate of 1 mV/s.

3. RESULTS AND DISCUSSION

The microstructure observations were performed after preparation of the specimens according to the standard procedure, i.e., grinding, polishing, and etching the surfaces. The results of the analysis for each specimen are presented in Fig. 1 – Fig. 7. SEM micrographs of the FSPed zone of each type specimen at 1000x magnification are shown (Fig. 1 a, Fig. 7 a). The locations where the distribution of Ti (Fig. 2 b, Fig. 3 b, Fig. 4 b) or Zn reinforcing particles (Fig. 5 b, Fig. 6 b, Fig. 7 b) was studied by EDS analysis is also shown, and the distribution of Ti and Zn particles was mapped (Fig. 2 c, Fig. 7 c). The microstructure of the FSPed zone in the reference specimen BA was uniform. Pores and cracking were not observed (Fig. 1 a). In specimens CTi2, CTi4, CTi6 (Fig. 2 a, Fig. 3 a, Fig. 4 a) containing 2, 4, and 6 mass % Ti respectively, the microstructure is visibly refined. The EDS analysis reveals uneven distribution of Ti and Ti-phases in the zone of stirring. Ti segregates and separates along the boundaries of the zone of FSP and Al-matrix (the purple particles in Fig. 3 c, Fig. 4 c).

The distribution of the reinforcing particles in the FSPed zone of CZn2, CZn4, and CZn6 (Fig. 5 a, Fig. 7 a), containing 2, 4, and 6 mass % Zn, respectively, is uneven and layered (Fig. 5 c, Fig. 7 c).

Surface-open pores are observed in the mixing zones of the samples shown in Fig. 7 b, although their size and depth were not quantitatively measured. No pores were detected in the other composite types. In our previous study [24], we demonstrated that the effect of pores on corrosion cannot be evaluated solely by their size or quantity, but rather as an interplay between the composite's architecture

and chemical composition. We examined Al-based composites with identical compositions but varying pore sizes and found that, when reinforced with Al_2O_3, composites with larger pores corrode more slowly than those with smaller pores, due to enhanced passive film stability. Conversely, in SiC-reinforced composites, larger pores intensify the activity of corrosion micro-galvanic cells between the reinforcing particles and the aluminum matrix, accelerating corrosion compared to composites with smaller pores. This finding, emphasizing the need for a comprehensive assessment of pore effects, is confirmed in the present study. The underlying reasons for the increased corrosion rate in this case are discussed further below. The EDS analysis reveals layers in the zone of stirring of CZn6 (Fig. 7 c) in which Zn is completely absent. The Zn content in other FSPed regions of CZn6 varies within the range 0.10 – 8.02 mass %.

FSP is a thermomechanical process in which the material flows around the tool at elevated temperature with a deformation rate in the range from 10 s^{-1} to 100 s^{-1} [13, 25] reaching effective strains in excess of 40 % [26], which are prerequisites for the separation of different phases. In the zones of stirring of composites CTi2, CTi4, and CTi6 (Fig. 8 a,) the XRD analysis identifies phases of Al(Cu, Mg) and Al3Ti, as well as peak concentrations of the reinforcing Ti particles. As the concentrations of reinforcing Ti particles increase, the intensity of the peaks of phase Al(Cu,Mg)-phase increases too. The Al3Ti-phase is identified only in composite CTi4. In the zones of stirring of composites CZn2, CZn4, and CZn6 only peaks of the main phase Al(Cu,Mg) are identified, as well as peaks of Zn particles concentration in CZn2 and CZn4 (Fig. 8 b). There is no indication of Al-Zn alloy formation or Zn segregation at grain boundaries that could affect corrosion.

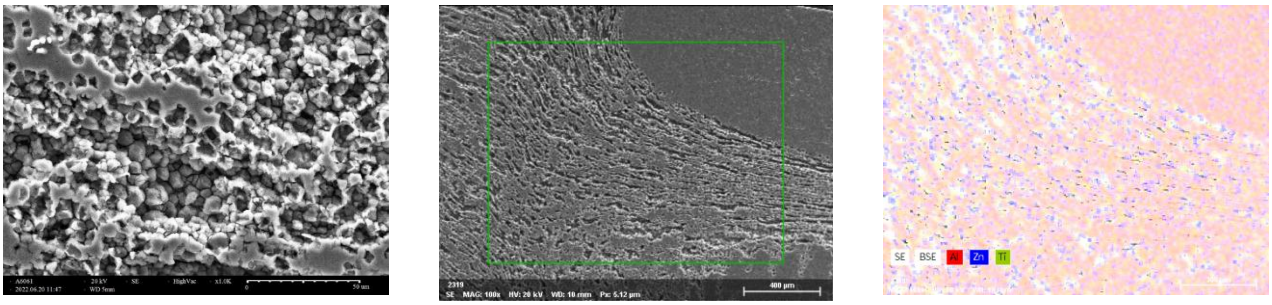

a b c

Fig. 1. Microstructure and chemical analysis of the FSP zone of Al6061 T6 BA: a – SEM micrograph of the FSP zone; b – EDS-analyzed area; c – EDS element distribution map

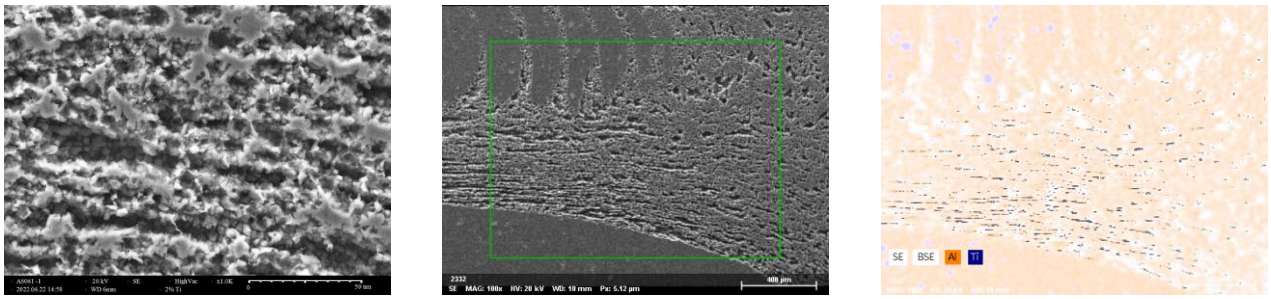

a b c

Fig. 2. Microstructure and chemical analysis of the FSP zone of Al6061 T6 + 2 mass % Ti: a – SEM micrograph of the FSP zone; b – EDS-analyzed area; c – EDS element distribution map

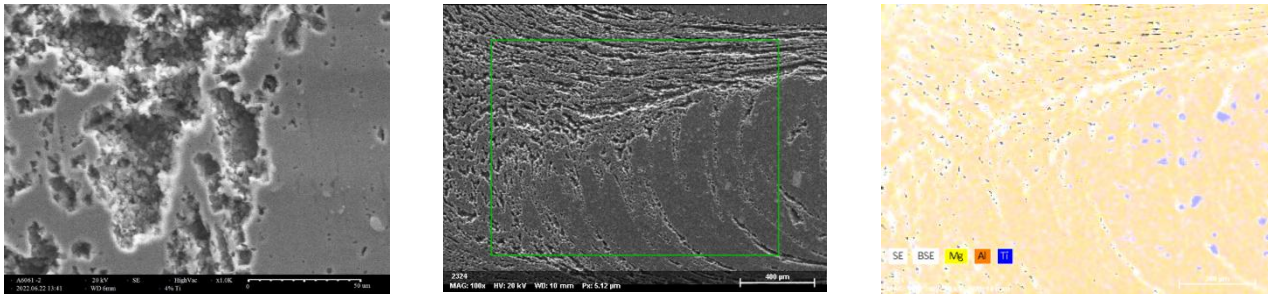

a b c

Fig. 3. Microstructure and chemical analysis of the FSP zone of Al6061 T6 + 4 mass % Ti: a – SEM micrograph of the FSP zone; b – EDS-analyzed area; c – EDS element distribution map

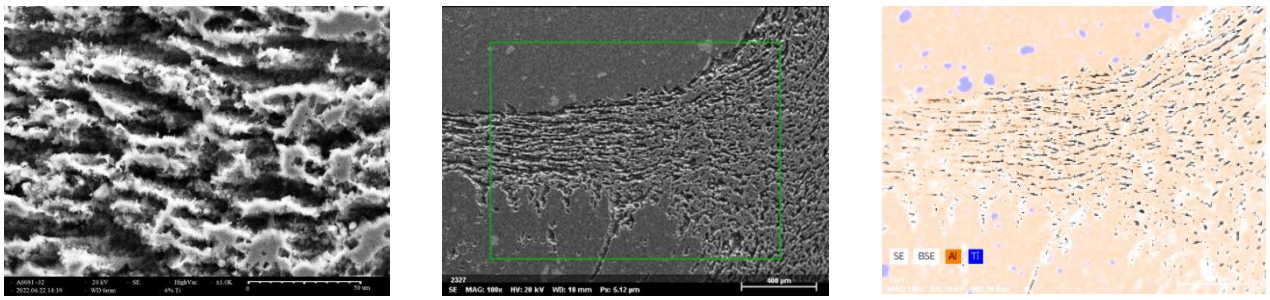

a b c

Fig. 4. Microstructure and chemical analysis of the FSP zone of Al6061 T6 + 6 mass % Ti: a – SEM micrograph of the FSP zone; b – EDS-analyzed area; c – EDS element distribution map

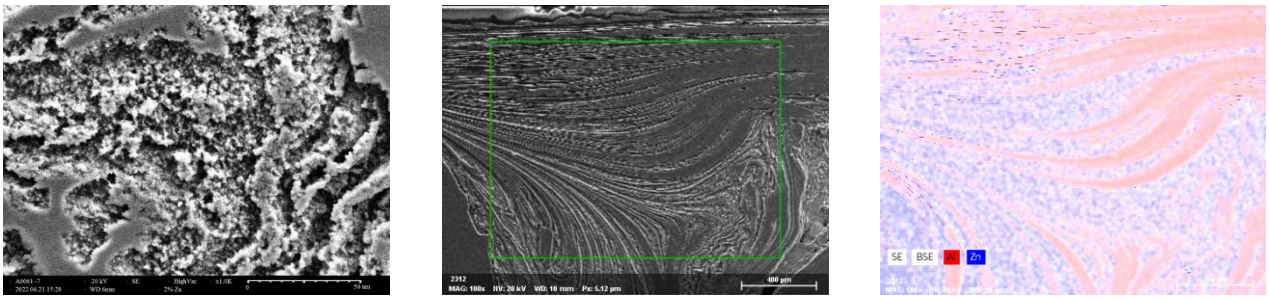

a b c

Fig. 5. Microstructure and chemical analysis of the FSP zone of Al6061 T6 + 2 mass % Zn: a – SEM micrograph of the FSP zone; b – EDS-analyzed area; c – EDS element distribution map

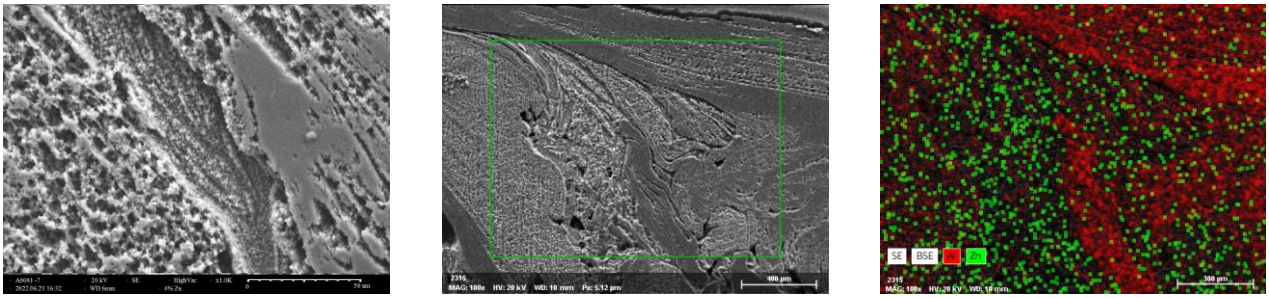

a b c

Fig. 6. Microstructure and chemical analysis of the FSP zone of Al6061 T6 + 4 mass % Zn: a – SEM micrograph of the FSP zone; b – EDS-analyzed area; c – EDS element distribution map

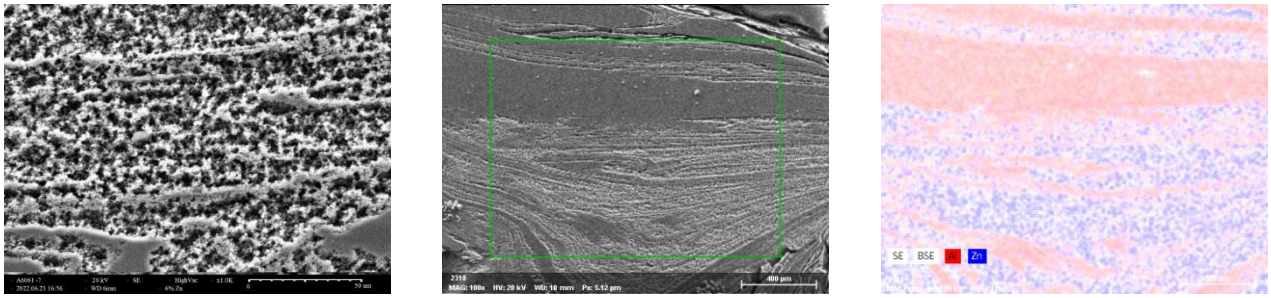

a b c

Fig. 7. Microstructure and chemical analysis of the FSP zone of Al6061 T6 + 6 mass % Zn: a – SEM micrograph of the FSP zone; b – EDS-analyzed area; c – EDS element distribution map

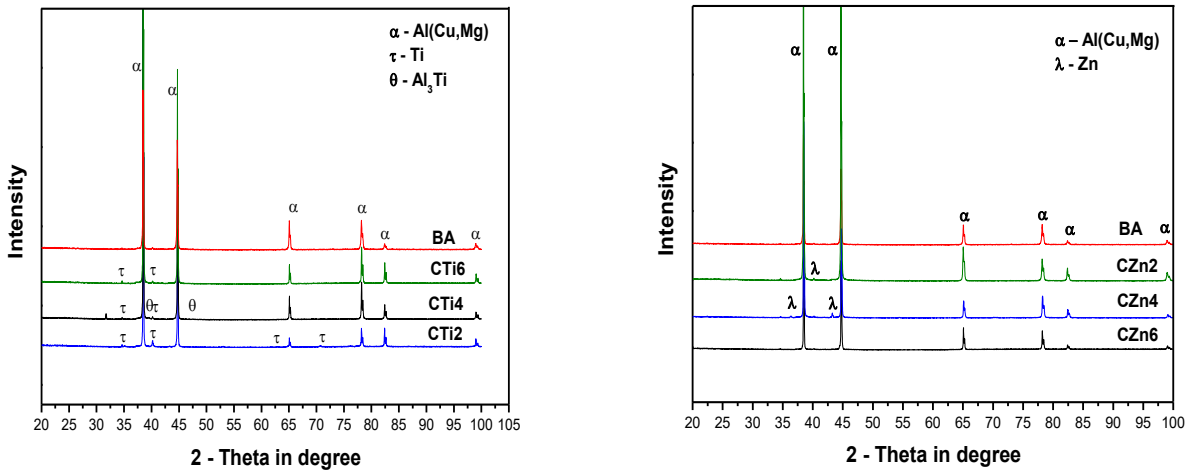

a b

Fig. 8. XRD patterns of composites reinforced with: a – Ti particles; b – Zn particles

The results for the calculated mass loss and the uncertainty after IGC tests, as well as the sustainability assessment according to ASTM G67 are presented in Table 1.

Table 1. Assessment of the corrosion resistance of AMCs reinforced with Ti and Zn particles

Designation of specimens	Reinforcing element, mass %	Mass loss, mg.cm^{-2}	Assessment according to ASTM G67
BA	0	1.67 ± 0.3	Sustainable
CTi2	2% Ti	2.21 ± 0.4	Sustainable
CTi4	4% Ti	2.47 ± 0.5	Sustainable
CTi6	6% Ti	1.72 ± 0.3	Sustainable
CZn2	2% Zn	3.46 ± 0.4	Sustainable
CZn4	4% Zn	3.58 ± 0.4	Sustainable
CZn6	6% Zn	9.08 ± 0.6	Slightly sensitive

According to the standard practice of ASTM G67, the mass loss should be within the range 1 – 8 mg.cm^{-2} with measurement uncertainty of 0.2 ± 3.9, mg.cm^{-2}. All samples except CZn6 prove to be resistant to IGC, as the reference alloy BA having the highest IGC resistance (lowest mass loss) equal to 1.67 mg.cm^{-2}.

The Ti-reinforced composites show better IGC resistance (less mass loss) compared to the Zn-reinforced specimens. Composite CTi6 shows IGC resistance almost equal to that of the reference alloy A6061 T6 (specimens BA). With increasing the concentration of Zn particles, there is a general decrease in IGC resistance, which is lowest in composite CZn6. In this case, the mass loss is 5 times greater than the mass loss of the reference alloy A6061 T6 and composite CTi6.

The IGC penetration was visually assessed, too. Fig. 9 shows micrographs of the cross-sections of the IGC test specimens after immersion in c. HNO_3 for 24 hours. The visual evaluations confirm the results of the gravimetric tests. The surface of specimen BA (Fig. 9 a) is smooth, without corrosion penetration into the depth of the specimen or disintegration of the composite grains. The specimens reinforced with 2, 4, and 6 mass % Ti also do not show the typical changes for IGC (Fig. 9 b, c, d). The surfaces are smooth, without corrosion penetration and grain fallout. There are insignificant surface changes on the cross-section of specimens CZn2 and CZn4 (Fig. 9 e, f). The roughness of the surfaces is most likely due to the FSP treatment and the reinforcing Zn particles, which are almost three times larger than the Ti particles. The surface of specimen CZn6 (Fig. 9 g) is strongly streaked due to the development of IGC.

The results for the main electrochemical characteristics, i.e., open circuit potential (OCP), corrosion potential (E_{corr}) and pitting potential (E_{pit}), obtained from the cyclic potentiostatic curves, are shown in Fig. 10 and Fig. 11. OCP dependence on time provides information about the corrosion behaviour of the studied material without the need for external polarisation [27]. OCP of specimens CTi2, CTi6, and CZn2 (blue, purple, and dark green lines in Fig. 10 a, respectively) show a positive change during the first 10-20 minutes of the test and subsequent stabilization. OCP of specimens CZn6 and BA (light green and red lines, respectively) is constant throughout the duration of the test. The higher OCP values of BA and CTi6 compared to the other tested composites indicate their ability to form good protective surface films [27].

The polarization dependencies of all studied composites, shown in Fig. 10 b, are characterized with a wide cathodic region. The reference alloy A6061 T6 has the lowest corrosion potential E_{corr} (-0.640 V) (Fig. 11 b). The other specimens show a shift in Ecorr in the cathodic region relative to E_{corr} of A6061 T6, with the Ti-reinforced composites showing a negligible shift of about 0.20 V, while the Zn-reinforced composites show a shift of about 0.300 V.

The cyclic polarization curves of BA and Ti- or Zn reinforced composites show sensitivity to local corrosion (Fig. 10 b). The positive hysteresis in all polarization curves indicates for development of pitting corrosion. The greater difference between the standard potentials of Al (1.676 V) and Zn (-0.762 V) compared to that of Al and Ti (1.210 V) [28] is a prerequisite for the greater tendency of Zn-reinforced composites to pitting corrosion. The hysteresis of the reference alloy BA and composites CTi2 and CTi6 is more pronounced than those of composites CZn2 and CZn6.

The shift in Epit for different types and concentrations of the reinforcing particles is shown in Fig. 11 a.

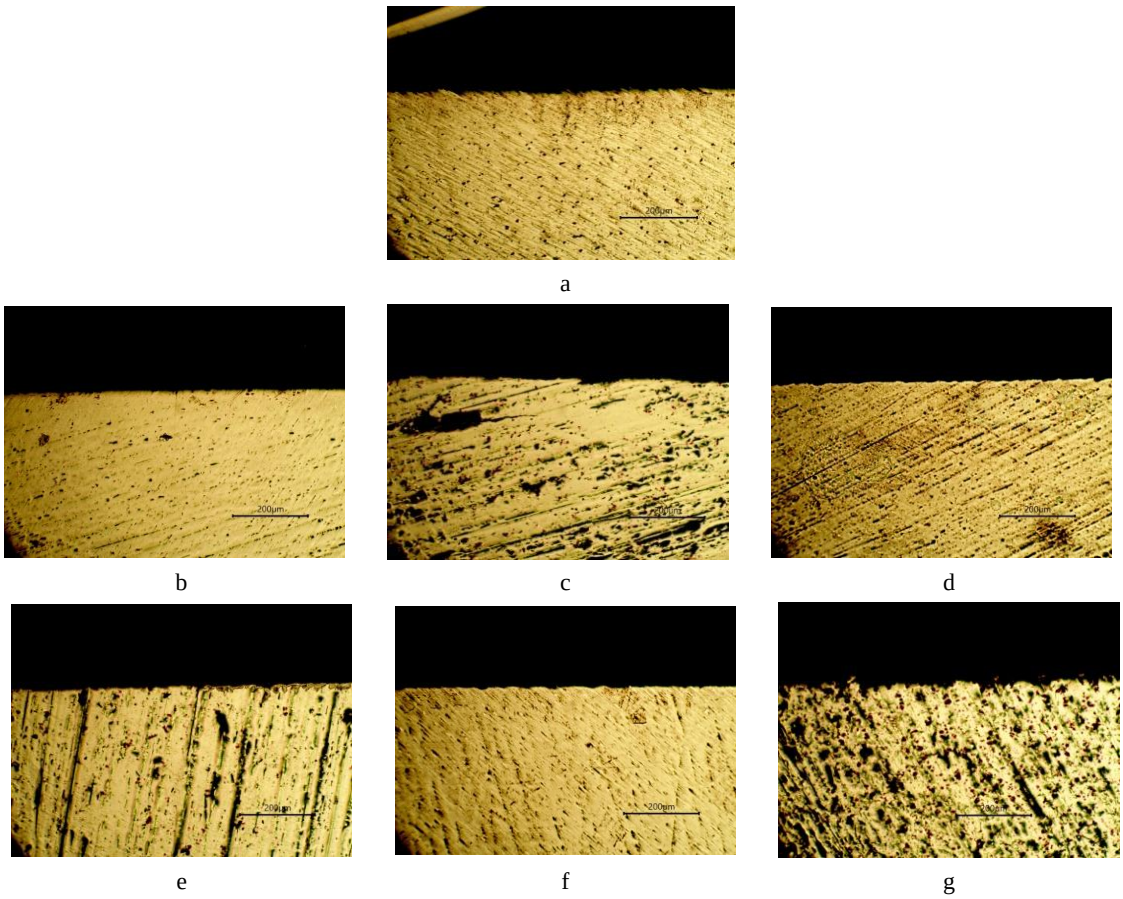

Fig. 9. Cross sections of the IGC tested specimens: a – reference alloy BA; b – composite CTi2; c – composite CTi4; d – composite CTi6; e – composite CZn2; f – composite CZn4; g – composite CZn6

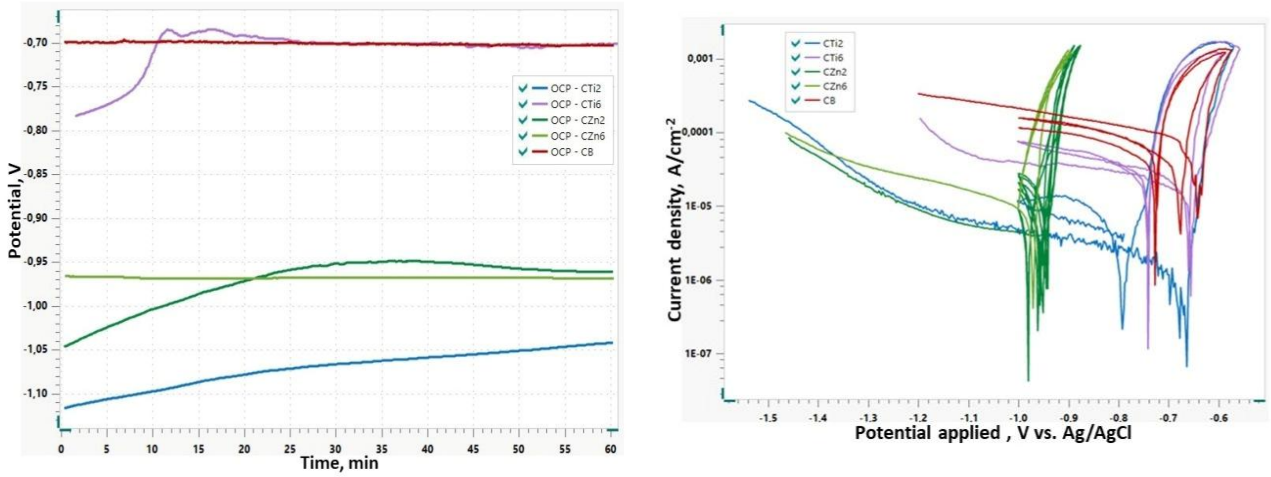

a b

Fig. 10. Ti- and Zn reinforced A6061 T6 composites: a – OCP curves; b – cyclic polarization curves

The pitting potentials of the reference alloy BA (-0.575 V) and composites CTi2 (-0.568) and CTi6 (-0.558 V) are more positive than those of Zn-reinforced composites CZn2 (-0.877 V) and CZn6 (-0.894 V), which is indicative for a better resistance to pitting. With increasing the Ti concentration, the pitting corrosion resistance of the composites improves.

Phases Al(Cu,Mg) and Al3Ti separated during FSP have a cathodic relation with respect to the anodic Al-alloy matrix and form microgalvanic elements, which are potential sources for the development of local corrosion [29]. In Ti-reinforced composites, the corrosion process is less pronounced, with corrosion behaviour very close to that of the reference alloy BA. It is known that in aluminium alloys alloyed with Ti, Ti and Al form an adhesive, protective oxide layer of Al_2O_3, as well as a mixed TiO_2-Al_2O_3 layer [30]. The barrier film formed on Ti-reinforced composites is thicker and more stable than that formed on pure aluminium, making it more resistant to corrosion. TiO_2 is stable, has insulating properties, and is non-conductive,

which decreases the rate of anodic dissolution [31, 32]. Evidence of the increased corrosion resistance of Ti-containing composites can be seen in the shift of the OCP of CTi6 towards the most positive values compared to the other studied composites (Fig. 10 a).

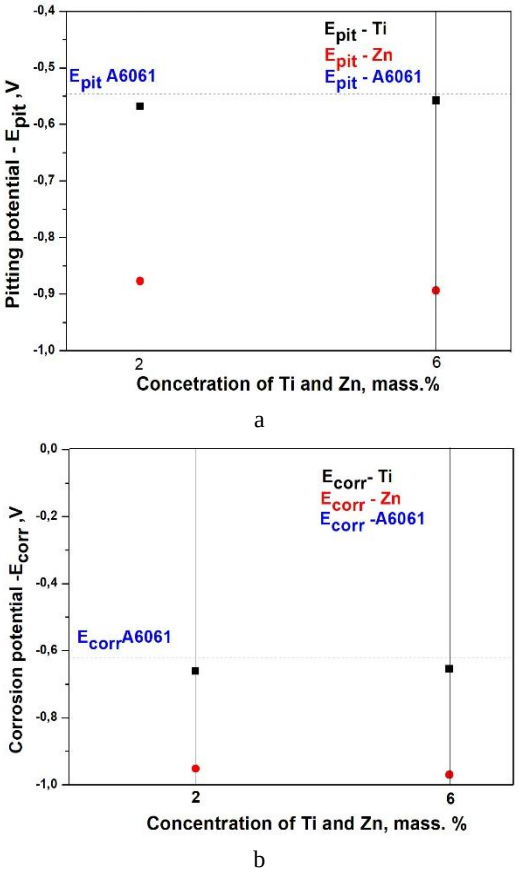

Fig. 11. Ti- and Zn reinforced A6061 T6 composite: a – corrosion potential E_{corr}; b – Pitting potential E_{pit}

In this case, adding 6 % titanium to the aluminium alloy shifts the OCP towards more positive values compared to the OCP values of Zn-reinforced composites and the reference BA alloy.

As expected, the corrosion of Zn-reinforced composites is accelerated for several reasons. The main reason is the cathodic behaviour of zinc particles in relation to the anodic aluminium matrix. Their larger size and concentration enhance the electrochemical interaction effect between them and the matrix. Another reason is FSP technology, which involves an asymmetric flow of material in the mixing zone, as well as the combined effect of different degrees of deformation and temperatures during FSP [4, 22, 23]. This leads to an uneven distribution of Zn particles (see Fig. 5, Fig. 6 and Fig. 7). Thirdly, the pores formed during FSP in the mixing zone (Fig. 7 b) increase the active electrochemical surface area, thereby enhancing the corrosion process. This intensifies the anodic dissolution process and increases the amount of corrosion product released, resulting in a loss of mass per unit area according to ASTM G67.

Therefore, although reinforcement with Ti and Zn particles improves the wear resistance and strength of A6061 T6-based composites obtained by FSP, products made from these composites are not recommended for use in environments containing aggressive ions.

Our future research will focus on several directions: optimizing the FSP process parameters to minimize pore formation that promotes corrosion; optimizing the type and concentration of added particles and evaluating their influence on the mechanical properties and corrosion resistance of aluminium composites; and conducting long-term testing of novel composite types in various corrosive environments.

4. CONCLUSIONS

The following conclusions can be drawn from the corrosion studies performed on Ti- and Zn- reinforced alloy A6061 T6-based AMCs obtained by friction stir processing:

In both types of alloy A6061 T6-based aluminium matrix composites reinforced with Zn- and Ti particles, corrosion processes by microgalvanic mechanism.

Alloy A6061 T6-based AMCs reinforced with Zn- and Ti particles are resistant to intergranular corrosion, but are susceptible to pitting corrosion.

Ti-reinforced AMCs are more resistant to pitting corrosion. They have a more positive pitting potential compared to the reference alloy A6061 T6 and the Zn-reinforced AMCs.

Despite the good wear resistance, Zn-reinforced AMCs are not recommended for applications in environments containing aggressive ions.

Acknowledgments

This work was supported by European Regional Development Fund under "Research Innovation and Digitization for Smart Transformation" program 2021-2027 under the Project BG16RFPR002-1.014-0006 "National Centre of Excellence Mechatronics and Clean Technologies".

REFERENCES

1. **Chak, V., Chattopadhyay, H., Dora, T.L.** A Review on Fabrication Methods, Reinforcements and Mechanical Properties of Aluminum Matrix Composites *Journal of Manufacturing Processes* 56 2020: pp. 1059 – 1074. https://doi.org/10.1016/j.jmapro.2020.05.042
2. **Samal, P., Vundavilli, P.R., Meher, A., Mahapatra, M.M.** Recent Progress in Aluminum Metal Matrix Composites: A Review on Processing, Mechanical and Wear Properties *Journal of Manufacturing Processes* 59 2020: pp. 131 – 152. https://doi.org/10.1016/j.jmapro.2020.09.010
3. **Mabuwa, S., Msomi, V., Ndube-Tsolekile, N., Zungu, V.M.** Status and Progress on Fabricating Automotive-Based Aluminium Metal Matrix Composites Using FSP Technique *Materials Today: Proceedings* 56 2022: pp. 1648 – 1652. https://doi.org/10.1016/j.matpr.2021.10.179
4. **Singh, H., Singh Brar, G., Kumar, H., Aggarwal V.** A Review on Metal Matrix Composite for Automobile Applications *Materials Today: Proceedings* 43 2021: pp. 20 – 325. https://doi.org/10.1016/j.matpr.2020.11.670

5. **Anish, R., Singh, G.R., Sivapragash, M.** Techniques for Processing Metal Matrix Composite: A Survey *Procedia Engineering* 38 2012: pp. 3846 – 3854. https://doi.org/10.1016/j.proeng.2012.06.441
6. **Hashim, J., Looney, L., Hashmi, M.S.J.** Metal Matrix Composites: Production by the Stir Casting Method *Journal of Materials Processing Technology* 92 – 93 1999: pp. 1 – 7. https://doi.org/10.1016/S0924-0136(99)00118-1
7. **Yadav, D., Bauri, R.** Friction Stir Processing of Al-TiB2 In Situ Composite: Effect on Particle Distribution Microstructure and Properties *Journal of Materials Engineering and Performance* 24 2015: pp. 1116 – 1124. https://doi.org/10.1007/s11665-015-1404-6
8. **Maz, Y.** Friction Stir Processing Technology: A Review *Metallurgical and Materials Transactions A* 39 2008: pp. 642 – 658. https://doi.org/10.1007/s11661-007-9459-0
9. **Ramanjaneyulu, K., Madhusudhan Reddy, G., Venugopal Rao, A.** Structure-Property Correlation of AA2014 Friction Stir Welds: Role of Tool Pin Profile *Journal of Materials Engineering and Performance* 22 2013: pp. 2224 – 2240. https://doi.org/10.1007/s11661-007-9459-0
10. **Arora, H.S., Singh, H., Dhindaw, B.K.** Composite Fabrication Using Friction Stir Processing – A Review *International Journal of Advanced Manufacturing Technology* 61 2012 pp. 1043 – 1055. https://doi.org/10.1007/s00170-011-3758-8
11. **Parikh, V.K., Badgujar, A.D., Ghetiya, N.D.** Joining of Metal Matrix Composites Using Friction Stir Welding: A Review *Materials and Manufacturing Processes* 34 2019: pp. 123 – 146. https://doi.org/10.1080/10426914.2018.1532094
12. **Radhiha, C.** Micro Structural Characteristics of Friction Stir Welded AA6061 Joint with TiB_2 and Al_2O_3 Particulate Reinforcements Addition *International Journal of Advanced Research in Engineering and Technology* 9 2020: pp. 1184 – 1197. https://doi.10.34218/IJARET.11.9.2020.118
13. **Mishra, R.S., Ma, Z.Y.** Friction Stir Welding and Processing *Materials Science and Engineering: R: Reports* 50 2005: pp. 1 – 78. https://doi.org/10.1016/j.mser.2005.07.001
14. **Zhang, Q., Xiao, B.L., Ma, Z.Y.** Mechanically Activated Effect of Friction Stir Processing in Al-Ti Reaction *Materials Chemistry and Physics* 139 2013: pp. 596 – 602. https://doi.org/10.1016/j.matchemphys.2013.01.062
15. **Yadav, D.R., Bauri Chawake, N.** Fabrication of Al-Zn Solid Solution via Friction Stir Processing *Materials Characterization* 136 2018: pp. 221 – 228. https://doi.org/10.1016/j.matchar.2017.12.022
16. **Kolev, M., Drenchev, L., Petkov, V., Dimitrova, R., Kovacheva, D.** Open-Cell AlSn6Cu-SiC Composites: Fabrication, Dry-Sliding Wear Behavior, and Machine Learning Methods for Wear Prediction *Materials* 16 2023: pp. 6208. https://doi.org/10.3390/ma16186208
17. **Kolev, M., Drenchev, L., Petkov, V., Dimitrova, R.** Production and Tribological Characterization of Advanced Open-Cell AlSi10Mg-Al_2O_3 Composites *Metals* 13 2023: pp. 131. https://doi.org/10.3390/met13010131
18. **Sharma, R., Singh, A., Arora, A., S. Pati, S., De, P.** Effect of Friction Stir Processing on Corrosion of Al−TiB2 Based Composite in 3.5 wt.% Sodium Chloride Solution *Transactions of Nonferrous Metals Society of China* 29 2019: pp. 1383 – 1392. https://doi.org/10.1016/S1003-6326(19)65045-4
19. **Soto-Diaz, R., Anderson, S.A., Gutierrez, J.E., Silgado, J.U.** Influence of Process Parameters on the Mechanical Properties and Corrosion Resistance of Dissimilar Friction Stir Welded Joints of AA2024-0 and AA6061-0 Aluminum Alloys *Metals* 14 (6) 2024: pp. 14060664. https://doi.org/10.3390/met14060664
20. **Jayakarthick, C., Povendhan, A.P., Vaira Vignesh, R., Padmanaban, R.** Analysing the Influence of FSP Process Parameters on IGC Susceptibility of AA5083 Using Sugeno – Fuzzy Model *IOP Conference Series: Materials Science and Engineering* 310 2018: pp. 012045. https://doi.org/10.1088/1757-899X/310/1/012045
21. **Valiev, R.Z., Murashkin, M.Y., Kilmametov, A.** Unusual Super-ductility at Room Temperature in an Ultrafine-grained Aluminum Alloy *Journal of Materials Science & Technology* 45 2010: pp. 4718 – 4724. https://doi.org/10.1007/s10853-010-4588-z
22. **Kondoff, Ch., Dykova, V., Dimitrova, R., Hadjitodorov Zaekova, Y.R.** 2021 A Layer Formation on 6061 Aluminum Alloy after FSP *International Journal, "NDT Days* IV 3 2021: pp. 178 – 186. www.bg-s-ndt.org/journal/vol4/JNDTD-v4-n3-a04.pdf
23. **Kondoff, Ch., Mikhov, R., Kirilov, L., Zaekova, R., Tashev, P.** Working Regimes for Friction Stir Processing of Aluminium Alloy A6061 *Environment. Technology. Resources. Proceedings* 3 2023: pp. 139 – 144. https://doi.org/10.17770/etr2023vol3.7235
24. **Kolev, M., Dyakova, V., Kostova, Y., Tzaneva, B., Spasova, H., Dimitrova, R.** Effects of Ceramic Particulate Type and Porosity on the Corrosion Behavior of Open-Cell AlSn6Cu Composites Produced via Liquid-State Processing *Metals* 15 2025: pp. 1073. https://doi.org/10.3390/met15101073
25. **Yadav, D., Bauri, R.** Effect of Friction Stir Processing on Microstructure and Mechanical Properties of Aluminium *Materials Science and Engineering: A* 539 2012: pp. 85 – 92. https://doi.org/10.1016/j.msea.2012.01.055
26. **Su, J.Q., Nelson, T.W., Sterling, C.J.** Microstructure Evolution during FSW/FSP of High Strength Aluminium Alloys *Materials Science and Engineering A* 405 2005: pp. 277 – 286. https://doi.org/10.1016/j.msea.2005.06.009
27. **Adamiak, M., Appiah, A.N.S., Wo´zniak, A., Nuckowski, P.M., Nazarov, S.A., Ganiev, I.N.** Impact of Titanium Addition on Microstructure, Corrosion Resistance, and Hardness of As-Cast Al+6%Li Alloy *Materials* 16 2023: pp. 2671. https://doi.org/10.3390/ma16072671
28. **Kurzweil, P.** BATTERIES/Nomenclature *Encyclopedia of Electrochemical Power Sources* 2009: pp. 381 – 394. https://doi.org/10.1016/B978-044452745-5.00042-3
29. **Tao, J.** Surface Composition and Corrosion Behavior of an Al-Cu Alloy. Chem. Phys. Université Pierre et Marie Curie – Paris V. English PA066159, 2016. https://theses.hal.science/tel-01412882/
30. **Hamza, A.H., Nama, A., Esen, I., Volkan Karakurt, A.H.** Effect of the Ti Addition on the Corrosion Behavior of Newly Developed AA7075-Ti Alloys *Journal of Alloys and Compounds* 969 2023: pp. 172349. https://doi.org/10.1016/j.jallcom.2023.172349

31. **Dias, V., Maciel, H., Fraga, M., Lobo, A.O., Pessoa, R., Marciano, F.R.** Atomic Layer Deposited TiO_2 and Al_2O_3 Thin Films as Coatings for Aluminum Food Packaging Application *Materials* 12 2019: pp. 682. https://doi.org/10.3390/ma12040682

32. **Kai, M., Rui, Z., Junlong, S., Changxia, L.** Oxidation Mechanism of Biomedical Titanium Alloy Surface and Experiment *International Journal of Corrosion* 2020 pp. 1 – 9. https://doi.org/10.1155/2020/1678615